The Flexible Accumulation Model for High Density Temporal Exposures

Xinkai Zhou¹, Lee Goeddel², Nauder Faraday², Ciprian M. Crainiceanu¹

Department of Biostatistics, Johns Hopkins University

Department of Anesthesiology and Critical Care Medicine, Johns Hopkins University

Abstract

Emerging technologies enable continuous monitoring of temporal exposures to disease risk factors, leading to complex structures in the exposure process that consists of a subject-specific number and duration of exposure episodes. A key scientific question is how does the number and duration of episodic exposure affect disease risk. We address this question by introducing the FLexible Accumulation ModEl (FLAME) and the associated inferential tools, whose finite sample performance is evaluated through comprehensive simulations. FLAME is motivated by and applied to quantifying the association between hypotensive exposure during cardiac surgery and acute kidney injury (AKI). Our results characterize the AKI risk accumulation pattern as a function of hypotensive duration and shows that while 60 one-minute episodes is associated with an AKI probability of 0.23, a single sustained sixty-minute hypotensive episode raises that probability to 0.32, a 37% increase despite the same total duration. These results offer direct guidance for improving hemodynamics risk management strategies during intraoperative care. Our method is accompanied by the R package flame.

Keywords: Hemodynamic data, time-varying exposure, risk accumulation, Bayesian inference, semiparametric regression

1 Introduction

Chronic and acute health conditions often result from time-varying exposures, including physiological, behavioral, or environmental risk factors. Understanding how risk accumulates over these time-varying exposures is critical for targeted interventions and personalized treatment. In cardiac surgery, for example, hemodynamic data such as mean arterial pressure (MAP) and central vein pressure (CVP) are continuously collected during surgical procedures and is associated with adverse health outcomes after surgery, such as acute kidney injury (AKI) (Goeddel et al., 2024). The patterns of exposure, however, are not defined a priori and can be highly heterogeneous across study participants, as we illustrate below.

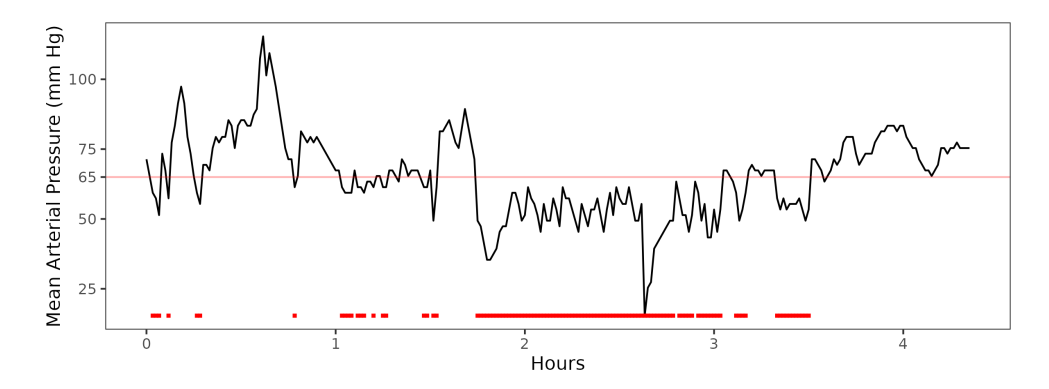


Figure 1: Mean arterial pressure (MAP) for a patient during cardiac surgery. Red bars at the bottom indicate episodes of hypotension, defined as MAP < 65 mm Hg.

Figure 1 displays the mean arterial pressure (MAP) expressed in millimeters of mercury (mm Hg) for a patient undergoing coronary artery bypass grafting (CABG). The x-axis represents time from the start of surgery, while the red horizontal line at 65 mm Hg indicates the threshold for hypotension. Below this line, the patient meets clinical consensus for hypotension. The red bars at the bottom of the figure represent the number and duration of hypotensive episodes. Two key observations emerge: (1) the patient repeatedly enters and exits the hypotensive state during surgery, creating multiple distinct episodes; and (2) these episodes vary in duration, from minutes to hours.

The scientific question is: how does the number and duration of the observed hypotensive events affect the risk of adverse health outcomes (e.g., AKI after surgery)? A first line approach is to use the total hypotensive time as a summary of exposure. However, such an approach would not distinguish between the risk of patients who accumulated the same total exposure but have different durations of contiguous minutes of exposure. For example, two patients may both have 60 minutes of hypotensive time, but one patient accumulated them through 60 isolated one-minute episodes while the other through an uninterrupted sixty-minute episode. The difference may seem to be of nuance, but the different patterns have different implications for clinical practice. For example, risk of organ injury may be non-linear with increasing duration of contiguous exposure, and interventions to manage hypotension could be more precisely administered based on duration of exposure over time. Unfortunately, analytic methods for addressing this important scientific issue do not currently exist.

To fill this gap, we propose the FLexible Accumulation ModEl (FLAME), which explicitly models risk accumulation at the episode-level. Therefore, the main novelty of the paper is to provide a new statistical framework that directly and precisely answers the scientific question of interest. The paper is organized as follows. Section 2 reviews the literature on methods for analyzing exposures. Section 3.1 introduces the FLAME method and its implementation. Section 4 presents simulation results evaluating FLAME's performance under diverse scenarios. Section 5 applies FLAME to hemodynamic data during cardiac surgery from the Johns Hopkins Hospital, revealing novel insights into AKI risk accumulation. Section 6 provides a discussion of the study's broader implications and future research directions.

2 Literature Review

Time-varying exposures are the de facto reality in many research domains, including pharmacoepidemiology (Rothman, Greenland, & Lash, 2008), environmental health (Nieuwenhuijsen, 2003), and cardiac surgery (Goeddel et al., 2024). Limitations in measurements and a need for translational models gave rise to a rich literature using summaries of time-varying exposures. For example, the weighted cumulative exposure (WCE) approach (Breslow, Lubin, Marek, & Langholz, 1983; Thomas, 1988) aggregates past exposures using a weighted sum, where the weights are either predetermined (Berry, Gilson, Holmes, Lewinsohn, & Roach, 1979; Vacek, 1997) or estimated (Hauptmann, Wellmann, Lubin, Rosenberg, & Kreienbrock, 2000). In cohort studies, WCE can be calculated at each follow-up time and then used in a Cox model as a time-dependent covariate (Sylvestre & Abrahamowicz, 2009; Y. Xiao, Abrahamowicz, Moodie, Weber, & Young, 2014). Generalized additive models allow for flexible modeling of scalar exposures (Crainiceanu, Ruppert, & Wand, 2005; Hastie & Tibshirani, 1986; Ruppert, Wand, & Carroll, 2003; Umlauf, Klein, & Zeileis, 2018; Wood, 2017) and recent advances allow many scalar exposures to be flexibly modeled together (Bai, Moran, Antonelli, Chen, & Boland, 2022; Hu et al., 2023; Lin & Zhang, 2006; Marra & Wood, 2011; Panagiotelis & Smith, 2008; Ravikumar, Lafferty, Liu, & Wasserman, 2009; Scheipl, Fahrmeir, & Kneib, 2012).

However, the data structure and the type of scientific questions have changed, requiring new inferential tools. For example, modern monitoring technologies provide data at much higher temporal resolutions, which raises questions about whether the mean (weighted or not) is sufficient to capture the underlying complexity of the exposure function. This led to new developments in functional data analysis (Crainiceanu, Goldsmith, Leroux, & Cui, 2023; Ramsay & Silverman, 2005), which consider the entire exposure function. In particular, scalar-on-function regression (SOFR) (Reiss, Goldsmith, Shang, & Ogden, 2017; Tikhonov, 1963; Wahba, 1990) and functional additive models (McLean, Hooker, Staicu,

Scheipl, & Ruppert, 2014; Müller & Yao, 2008) have been developed for exposures with the same domain (e.g., beginning to end of surgery) and the same interpretation of data at the same time point (e.g., percent time elapsed from the surgery). However, these models do not account for risk accumulation over exposure episodes (e.g., hypotension intervals) of a different number and duration. Some literature exists for transformations of episodic exposures (Vacek, 1997), but we are not aware of any general framework for directly estimating risk accumulation as a function of the number and duration of exposure episodes.

3 Methods

The data structure in this paper is the one suggested by the cardiac surgery example introduced in Section 1. Let Y_i for $i=1,\ldots,I$ be a scalar outcome of interest (e.g., AKI status) with an exponential family distribution and $\mathbf{X}_i = (X_{i1}, X_{i2}, \ldots, X_{ip})^t$ be a p-dimensional vector of baseline covariates (e.g., age and sex). Denote by J_i the number of exposure episodes, by $\mathbf{Z}_i = (Z_{i1}, \ldots, Z_{iL_i})^t$ the vector of lengths of exposure episodes (length of intervals), and by $\mathbf{S}_i = (S_{i1}, \ldots, S_{iL_i})^t$ the times when these exposure episodes occur. For example, in Figure 1, there were $J_i = 15$ episodes; the first episode started at minute $S_{i1} = 3$ of the surgery and lasted for $Z_{i1} = 3$ minutes; the longest episode was the 11th episode, started at minute $S_{i11} = 106$ of the surgery and lasted for $Z_{i11} = 63$ minutes. The observed data are of the form $(Y_i, \mathbf{X}_i, \mathbf{Z}_i, \mathbf{S}_i)$, where both \mathbf{Z}_i and \mathbf{S}_i are vectors of length J_i , which is subject-specific. Thus, the exposure does not have the same fixed domain and the FOSR methodology cannot be applied directly. The work on uneven functional domains (Gellar, Colantuoni, Needham, & Crainiceanu, 2014; Jordan T. Johns & Gellar, 2019) does not apply here, because the structure of our exposure function is different.

3.1 Flexible Accumulation Model

Our key modeling insight is that each episode contributes risk as an unknown function of its duration. Let $f(\cdot)$ be this function, which will be referred to as the *risk accumulation* function (RAF). We propose the following FLexible Accumulation ModEl (FLAME):

$$g\{\mathbb{E}[y_i]\} = \mathbf{X}_i \boldsymbol{\beta} + \sum_{j=1}^{J_i} f(Z_{ij}), \tag{1}$$

where $g(\cdot)$ is a canonical link function, $X_i\beta$ accounts for the risk associated with the person-specific covariates, and $\sum_{j=1}^{J_i} f(Z_{ij})$ is the sum of all individual risk on the linear predictor scale. To build up intuition, when $f(z) = z\gamma$ the accumulated risk is $\sum_{j=1}^{J_i} f(Z_{ij}) = (\sum_{j=1}^{J_i} Z_{ij})\gamma$, where $T_i = \sum_{j=1}^{J_i} Z_{ij}$ is the total exposure time for patient i. This means that using the total duration of exposure as a covariate in an ordinary generalized linear model (GLM) is a special case of FLAME when the RAF is assumed to be linear.

FLAME allows for different individuals with the same total duration of exposure to have different risk if the accumulation pattern is different. For example, for an individual with 60 episodes of one-minute exposure, the risk contribution is $\sum_{j=1}^{J_i=60} f(1) = 60 \times f(1)$. For another individual with 1 episode of sixty-minute exposure, the risk contribution is $\sum_{j=1}^{J_i=1} f(60) = f(60)$. If $f(60) > 60 \times f(1)$, we conclude that a sixty-minute episode is riskier than 60 one-minute episodes. FLAME also allows us to estimate $f(60) - 60 \times f(1)$, $f(60)/[60 \times f(1)]$, and $[f(60) - 60 \times f(1)]/f(1)$, all of which are measures of how much riskier a sixty-minute episode is compared to 60 one-minute episodes. Therefore, model (1) is designed to answer the specific scientific question described in Section 1. The RAF $f(\cdot)$ is modeled nonparametrically using penalized splines to provide greater flexibility in capturing complex shapes.

3.2 Parameter Estimation

We adopt a Bayesian estimation framework. For binary outcome, the model is:

$$\begin{cases} y_i \mid \boldsymbol{X}_i, \{z_{ij}\} & \sim \text{Bernoulli}\{p(\boldsymbol{X}_i, \{z_{ij}\})\}; \\ \log \operatorname{it}\{p(\boldsymbol{X}_i, \{z_{ij}\})\} & = \boldsymbol{X}_i \boldsymbol{\beta} + \sum_{j=1}^{J_i} f(z_{ij}); \\ f(z) & = \sum_{k=1}^{K} \gamma_k b_k(z). \end{cases}$$

The RAF is modeled using penalized splines where $b_k(z), k = 1, \dots, K$, are spline basis functions and $\gamma = (\gamma_1, \dots, \gamma_K)^t$ are corresponding spline coefficients. Specifically, we use cubic B-spline bases with equally-spaced knots spread across the range of exposure duration and impose a second order difference penalty (Eilers & Marx, 1996) on the spline coefficients γ through the random walk prior (Lang & Brezger, 2004) $\gamma_{k+2} \sim N(2\gamma_{k+1} - \gamma_k, \tau_{\gamma}^2)$ for k = 11,...,K-2. Here au_{γ} is the smoothing parameter and is assigned a half-Cauchy prior (Gelman, 2006). For γ_1 and γ_2 we assign priors half-Normal(0, 10^{-6}) and half-Normal(0, 1), respectively. We choose half-Normal instead of Normal to enforce non-negativity of RAF near 0, driven by the application-specific consideration that any hypotensive exposure, no matter how short, should be harmful. This constraint may not hold in other applications and can easily be removed by using Normal instead of half-Normal priors. The choice of a variance of 10^{-6} for γ_1 is to enforce the soft constraint that $f(0) \approx 0$ because physiologically, the risk of a zero-minute episode should be 0. We further assign independent diffuse normal priors to the fixed effect parameters β . An alternative to the second order difference penalty is the penalty on the integral of the squared second derivative of $f(\cdot)$ (Crainiceanu et al., 2005; Harezlak, Ruppert, & Wand, 2018; O'Sullivan, 1986; Ruppert et al., 2003; Wahba, 1990; Wand & Ormerod, 2008), which we do not use here.

Theoretical guarantees for penalized splines have been studied in both frequentist (Claeskens, Krivobokova, & Opsomer, 2009; Li & Ruppert, 2008; Schwarz & Krivobokova,

2016; L. Xiao, 2019; L. Xiao, Li, Apanasovich, & Ruppert, 2012) and Bayesian frameworks (Bach & Klein, 2025; de Jonge & van Zanten, 2012; Ghosal & van der Vaart, 2007; Yoo & Ghosal, 2016). Specifically, Bach and Klein (2025) showed that for Gaussian nonparametric regression, the posterior of Bayesian penalized splines concentrates at near optimal rate for O-splines under certain hyperpriors for the smoothing variance. We leave it to future work to explore the posterior concentration of the FLAME estimator.

To summarize, FLAME offers three key advantages. First, episodic modeling. By calculating $f(z_{ij})$, the RAF value for each episode, FLAME captures differences in exposure duration within the same subject, which cannot be modeled using existing methods. As mentioned above, a GLM with total duration as a covariate is a special case of FLAME when $f(\cdot)$ is assumed to be a linear function. Second, flexibility. FLAME encodes the idea that an underlying RAF governs how risk accumulates within each episode of exposure without assuming any specific functional form. Its estimation strategy inherits the flexibility of nonparametric modeling, reduces the risk of model misspecification, and is more likely to capture the true relationship between the exposure and outcome (Harezlak et al., 2018; Ruppert et al., 2003). Third, adaptability. While we assumed for simplicity that the same RAF governs the entire observation window (e.g., the entire surgery), it is plausible that different phases of cardiac surgery (e.g., before, during, or after cardiopulmonary bypass) may be governed by their own RAF. FLAME is adaptable and can be extended to allow for phase-specific RAF, an approach that will be explored in future work.

4 Simulation study

We conducted extensive simulations to examine FLAME's performance under various settings. Binary outcomes were generated from a model with linear predictor $logit(p_i) = X_i \beta + \sum_{j=1}^{J_i} f(z_{ij})$. We set $X_i \beta = -3.5 + 0.1 X_{i1}$ and $X_{i1} \sim N(0,1)$, which, under the assumption of no-exposure (number of exposure episodes $J_i = 0$), corresponds to a baseline

event rate around 3%. The number of episodes J_i was generated independently with equal probabilities in the set of integers $\{0, 1, ..., 15\}$; the duration of each exposure event z_{ij} was generated independently and uniformly on the interval (0, 30]. We varied the sample size $I \in \{1000, 2000, 5000\}$ and the number of basis functions $K \in \{30, 40, 50\}$. Four shapes were considered for the RAF $f(\cdot)$: linear, piecewise linear, logarithm, and sigmoid. Parameters of the RAF such as the slope of the linear RAF were chosen through trial and error to achieve event rates of 10%, 30%, and 50%, which is another simulation setting we considered. See Supplementary Materials Table 4 for the exact functions used.

To conduct inference we used MCMC sampling implemented in Stan and used four chains with 1000 warm up iterations and 2000 sampling iterations. There were a total of 108 simulation scenarios and 100 simulations for each scenario, leading to a total of 10,800 simulation experiments. The RAF estimator, $\hat{f}(z)$, was evaluated against the true RAF, f(z), using the integrated squared error (ISE) $\int_0^{30} {\{\hat{f}(z) - f(z)\}^2 dz}$.

4.1 Simulation Results

Figure 2 shows the estimated RAFs for various sample sizes for linear, piecewise linear, logarithm, and sigmoid shapes. The event rate was set to 30% and K = 30 cubic B-spline basis functions were used. In each panel, the red curve is the true function; black lines represent estimates from one-hundred simulated datasets.

The top row in Figure 2 indicates that FLAME successfully recovers the linear shape at all sample sizes considered. The second and third rows indicate that the piecewise-linear and exponential RAFs are also well approximated and approximations are getting better with increased sample size. The fourth row indicates that the sigmoid RAF was the most difficult to estimate, though estimation does improve for very large sample sizes.

We also examined how the sample size, I, and number of basis functions, K, affect RAF estimation. Table 1 summarizes the mean ISE across 100 simulation experiments

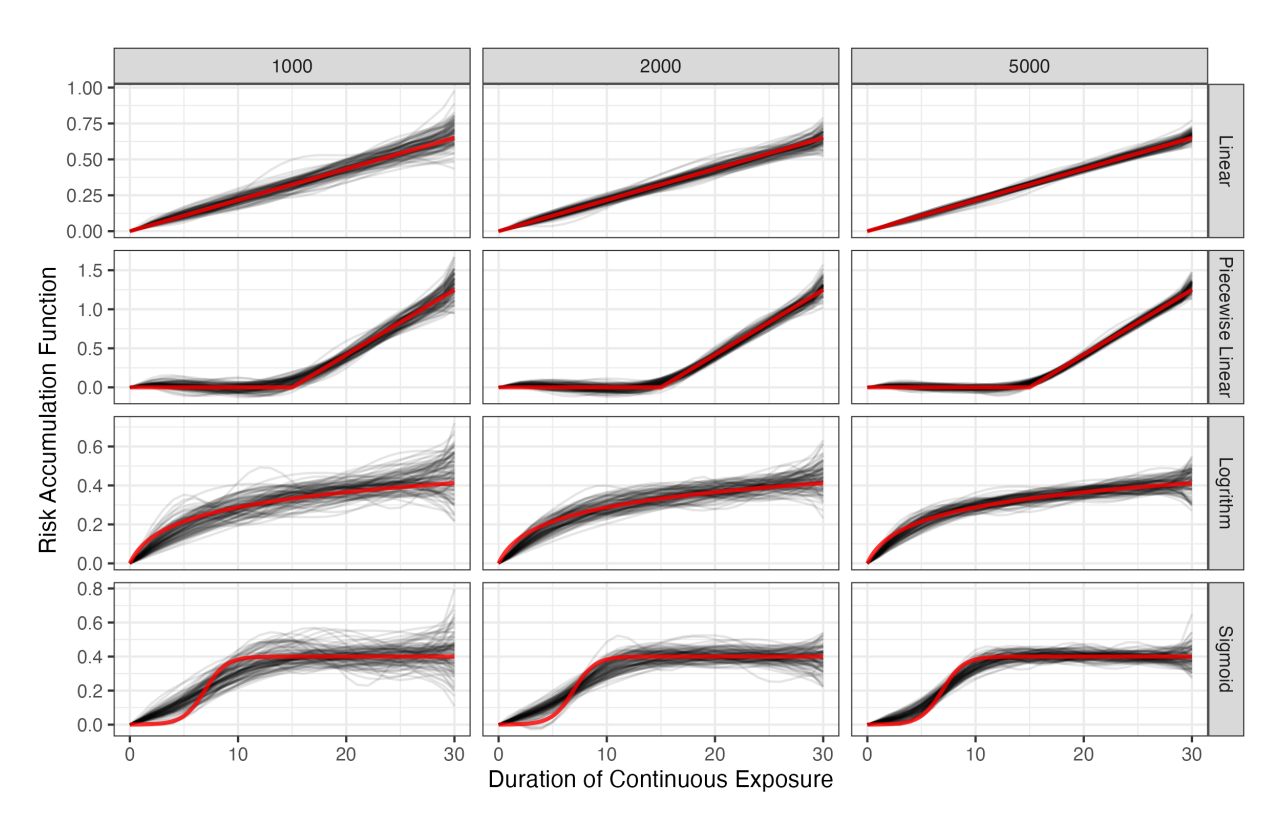


Figure 2: True RAF (red) versus estimates (black) from 100 simulated data sets for sample sizes I=1000,2000,5000 and various shapes (linear, piecewise linear, logarithm, and sigmoid). The event rate was fixed at 30% and the number of cubic B-spline basis functions was K=30.

	Linear			Piecewise Linear			Logarithm			Sigmoid		
K	1000	2000	5000	1000	2000	5000	1000	2000	5000	1000	2000	5000
30	0.046	0.020	0.008	0.121	0.062	0.033	0.080	0.041	0.022	0.118	0.067	0.034
40	0.040	0.020	0.009	0.123	0.065	0.034	0.063	0.041	0.020	0.104	0.072	0.032
50	0.041	0.017	0.009	0.111	0.057	0.030	0.061	0.037	0.021	0.100	0.068	0.035

Table 1: Mean integrated squared error (ISE) of RAF estimates across 100 simulation experiments at different shapes, sample size I, and number of basis functions K at the event rate of 30%. Differences in ISE is relatively small across different K for a given shape and sample size I, highlighting the robustness of FLAME to the choice of K.

for various simulation settings. The ISE decreases quickly as sample size increases. The differences in ISE is relatively small across different K for a given shape and sample size I. Furthermore, as the sample size grows, the difference in ISE between different K becomes smaller. Additional details, including computational time and results for event rates of 10% and 50% appear in the Supplementary Material Section 7.2.

5 Application

5.1 Data description

We applied FLAME to data from patients who underwent CABG surgery at the Johns Hopkins Hospital (JHH) between July 1, 2016 and October 31, 2019. Patients were included if they underwent isolated CABG with cardiopulmonary bypass (CPB). High frequency hemodynamic data for MAP was extracted from the electronic health record and matched to clinical variables available from the JHH Society of Thoracic Surgery (STS) database. The data set contains 1,199 patients and has been described in detail by Goeddel et al. (2024). The outcome of interest is acute kidney injury (AKI) at 48 hours after surgery as defined by the KDIGO criteria using change in serum creatinine (Khwaja, 2012).

From this initial data set we excluded eight patients who experienced at least one episode lasting more than 75 minutes because this was a very rare exposure. We also excluded three

	AKI No $(N = 858)$	AKI Yes $(N = 330)$
Age	64.0 (9.6)	65.6 (9.7)
Gender = Male (%)	673 (78.4)	247 (74.8)
Renal Failure Score	0.02(0.04)	0.05 (0.07)
Total Surgery Time	6.5 (1.2)	6.9(1.8)
Number of Episodes	11 (5)	11 (5)
Number $(\%)$ of subjects		
with at least one episode		
$\geq 10 \text{ minutes}$	577 (67.2)	252 (76.4)
$\geq 20 \text{ minutes}$	232 (27.0)	125 (37.9)
$\geq 30 \text{ minutes}$	82 (9.6)	72 (21.8)
$\geq 40 \text{ minutes}$	36 (4.2)	38 (11.5)
≥ 50 minutes	23(2.7)	19 (5.8)
$\geq 60 \text{ minutes}$	12 (1.4)	11 (3.3)

Table 2: Summary of the analytic sample. Gender and episode distribution are summarized as count (%). All others variables are summarized as mean (SD).

patients who are missing the STS renal failure score, a composite preoperative risk measure. After exclusion, our analytic sample included 1,188 patients, of whom 330 (28%) developed AKI within 48 hours after surgery.

The exposure is hypotension, a hemodynamic state defined as MAP less than 65 mm Hg. MAP is the average blood pressure during a single cardiac cycle, and is measured through catheters placed in the radial/femoral artery and recorded at 1-minute resolution during surgery. Total duration of hypotension during surgery has been reported to be associated with AKI (Scott & APSF Hemodynamic Instability Writing Group, 2024). It is not known, however, how AKI risk accumulates when patients enter the hypotensive state. For example, we would like to compare the risk of 60 one-minute hypotensive episodes with that of 1 sixty-minute hypotensive episode. We observed a total of 24,248 hypotensive episodes across study participants. The frequency and duration of hypotensive episodes and other patient characteristics are summarized in Table 2.

5.2 Analysis results

We applied FLAME to these data with adjustment for baseline covariates including the total surgery time and the STS predicted renal failure score, which is a composite score that encompasses a wide range of baseline demographic and risk factors for renal failure. We used K=30 B-splines bases to model the RAF and ran 4 MCMC chains with 1000 warm-up and 2000 sampling iterations. Figure 3 displays the estimated RAF (blue curve) and 95% credible intervals (gray area). The dashed line illustrates a linear extrapolation of the initial slope of the blue curve for comparison. Risk appears to accumulate linearly for episodes under 20 minutes, and the majority of hypotensive episodes were less than 20 minutes in duration. Indeed, only 2% of all episodes were 20 minutes or longer, but 357 patients had at least one such episode. The RAF estimate starts to rise faster than the linear rate for episodes longer than 20 minutes, suggesting that a continuous long episode poses higher risk compared to a sequence of short episodes of the same total duration. The confidence intervals become wider for episodes above 30 minutes and double in width for intervals of 60 minutes, most likely because the number of episodes of longer duration decreases substantially.

Conducting inference on RAF is straightforward using posterior samples. We illustrate this by addressing the clinical question raised in the introduction: is 1 sixty-minute episode riskier than 60 one-minute episodes? This can be answered by calculating the posterior distribution of $\operatorname{expit}[f(60)] - \operatorname{expit}[60 \times f(1)]$, where expit is the inverse logit function. As a sensitivity analysis, we conducted also the analysis with K = 20 and K = 40, and results were largely the same.

Table 3 provides the posterior means and 95% credible intervals of the estimated AKI probability for each scenario with K = 20, 30, 40. Across all models, a single continuous sixty-minute episode (f(60)) is associated with higher estimated AKI risk than 60 one-minute episodes $(60 \times f(1))$. For example, for K = 30 basis functions, 60 one-minute

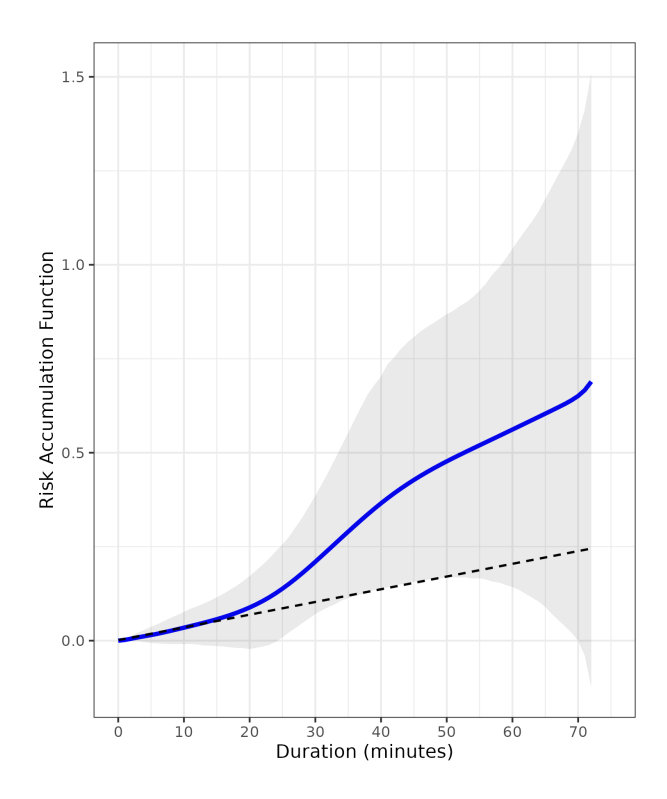


Figure 3: Estimated AKI risk accumulation functions (blue line) using FLAME for duration of hypotension with K=30 B-spline bases. The gray shaded region denotes the 95% credible intervals. The dashed line illustrates a linear extrapolation of the initial slope for comparison. The RAF estimate suggests that AKI risk accumulates faster than linear beyond 20 minutes of continuous hypotension.

episodes increases AKI probability from a baseline of 0.21 corresponding to no hypotensive episodes to 0.23. In contrast, a sixty-minute episode increases this probability to 0.32, a difference of 0.09 (95% CI: [0,0.21]). Despite the lack of statistical significance, which may be the result of insufficient power due to the moderate sample size, the point estimate is consistent across different K. The similarity in the estimated expected log predictive density (ELPD) statistics (Vehtari, Gelman, & Gabry, 2017) indicate similar fit across different numbers of B-spline basis.

6 Discussion

We proposed FLAME, a novel semiparametric model for directly estimating the risk accumulation pattern for time-varying exposures. By mapping each episode's duration through

	Number of B-spline basis						
Scenario	K = 20	K = 30	K = 40				
A (No hypotensive episode) B (60 one-minute episodes) C (1 sixty-minute episode)	0.21 (0.17, 0.26) 0.23 (0.17, 0.3) 0.32 (0.19, 0.5)	0.21 (0.17, 0.26) 0.23 (0.17, 0.31) 0.32 (0.19, 0.5)	0.21 (0.17, 0.26) 0.24 (0.17, 0.33) 0.32 (0.19, 0.5)				
B versus C (C - B)	0.09 (0, 0.21)	0.09 (0, 0.2)	0.09 (-0.01, 0.2)				
ELPD Estimate (SE)	-664.4 (16.9)	-664.6 (16.9)	-664.6 (16.9)				

Table 3: Estimated AKI probabilities and 95% credible intervals based on FLAME and three scenarios at different numbers of B-spline bases K. The estimated expected log predictive density (ELPD) via LOO-CV suggests similar fit across K.

a nonparametrically estimated RAF, FLAME avoids collapsing continuous exposures into a single scalar metric such as total duration. The model is especially relevant when physiological, clinical, or environmental knowledge supports the notion that prolonged continuous exposure to a risk state may be associated with different risk than fragmented or intermittent exposures.

Simulations confirm FLAME's ability to recover the true RAF across a broad range of shapes, event rates, sample sizes, and number of basis. Our real-data application to hypotension during CABG surgeries reveals clinically meaningful patterns, indicating that prolonged hypotension beyond 20 minutes is associated with disproportionately higher AKI risk. Such findings have direct implications for intraoperative blood-pressure management, where clinicians might consider more aggressive interventions if patients remain hypotensive beyond a particular duration. It is also worth noting that while our analysis focused on the duration of hypotension, the proposed framework can be readily extended to incorporate intensity of hypotension. For example, we can estimate the RAF for the exposure of "area under the hypotensive threshold of 65 mm Hg", which naturally incorporates both the duration and intensity of hypotension.

FLAME is an adaptive modeling framework that can be extended to accommodate multiple RAFs, for example, to capture differences in risk accumulation patterns during different phases of surgery. Additionally, it can be extended to accommodate multivariate

Shape	Event Rate	RAF
Linear	10%	0.03 / 3 * x
Linear	30%	0.065 / 3 * x
Linear	50%	0.1 / 3 * x
Piecewise Linear	10%	$0.1 / 3 * (x - 15) * 1_{\{x > 15\}}$
Piecewise Linear	30%	$0.25 / 3 * (x - 15) * 1_{\{x>15\}}$
Piecewise Linear	50%	$0.45 / 3 * (x - 15) * 1_{\{x>15\}}$
Logarithm	10%	$0.06 * \log(x + 1)$
Logarithm	30%	$0.12 * \log(x + 1)$
Logarithm	50%	$0.2 * \log(x + 1)$
Sigmoid	10%	$0.2 / (1 + 1000 * \exp(-x))$
Sigmoid	30%	$0.4 / (1 + 1000 * \exp(-x))$
Sigmoid	50%	$0.6 / (1 + 1000 * \exp(-x))$

Table 4: RAFs used in simulation experiments.

RAFs to model, for example, how combined hypotension and low cardiac output might interactively affect AKI risk. Further work is needed to study these approaches. Finally, although we implemented FLAME within a Bayesian framework, frequentist analogs using penalized splines are also possible.

In conclusion, FLAME provides a flexible and robust new approach for studying timevarying risk accumulation. Our results underscore how recognizing the episodic nature of exposures can significantly enhance scientific insights, opening paths to improved clinical decision-making and public health interventions.

7 Supplementary Materials

7.1 RAF for simulation

Table 4 shows the RAFs used in simulations under various shapes and event rates.

7.2 More simulation results

Figure 4 shows the mean computational time across 100 simulation experiments as a function of sample size for various number of basis functions K and RAF shapes. In this plot we fixed the event rate at 30%. We see that as sample size increases, computational time increases linearly, demonstrating the scalability of FLAME to large data sets.

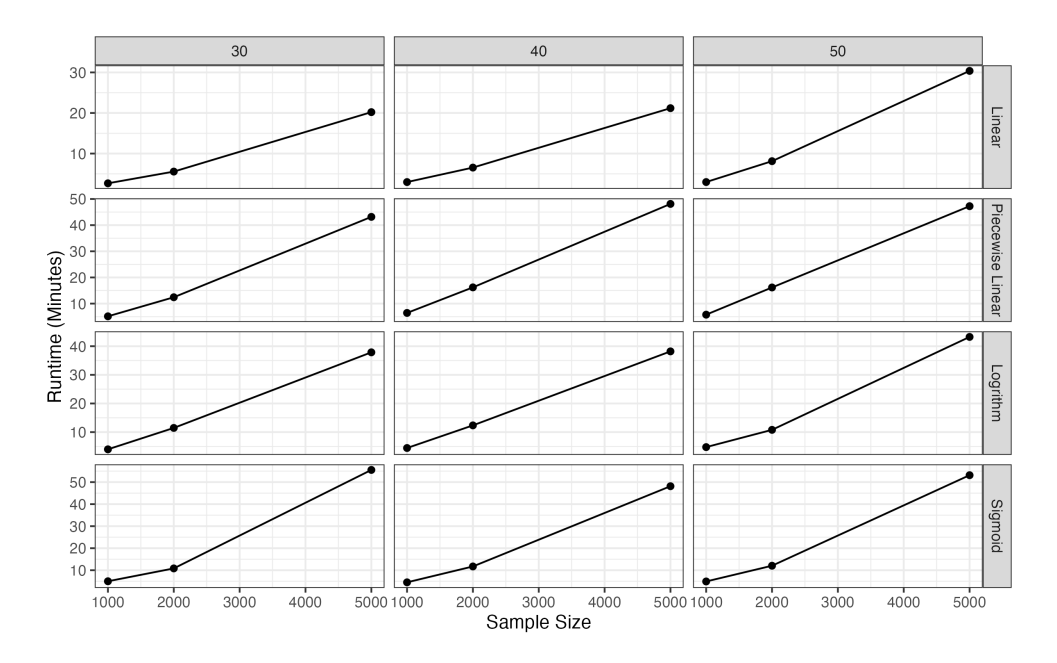


Figure 4: Mean computational time across 100 simulation experiments as a function of sample size for various number of basis functions K and RAF shapes. The event rate was fixed at 30%.

	Linear			Piecewise Linear			Logarithm			Sigmoid		
K	1000	2000	5000	1000	2000	5000	1000	2000	5000	1000	2000	5000
30	0.045	0.027	0.011	0.112	0.066	0.027	0.073	0.038	0.021	0.091	0.055	0.031
40	0.055	0.022	0.011	0.116	0.060	0.024	0.064	0.042	0.020	0.087	0.045	0.031
50	0.049	0.025	0.009	0.102	0.064	0.026	0.097	0.040	0.021	0.087	0.056	0.030

Table 5: Mean integrated squared error (ISE) of RAF estimates across 100 simulation experiments at different shapes, sample size I, and number of basis functions K at the event rate of 10%.

Table 5 and 6 show the mean ISE across 100 simulation experiments at the event rate of 10% and 50%. Similar to the setting of 30% event rate, we observe fast decline in ISE as sample size increases and relatively small differences in ISE across different K. Since the RAFs for different event rates are on different scales (Table 4), comparison of ISE is only warranted for the same event rate.

	Linear			Piecewise Linear			Logarithm			Sigmoid		
K	1000	2000	5000	1000	2000	5000	1000	2000	5000	1000	2000	5000
30	0.071	0.038	0.015	0.317	0.169	0.073	0.145	0.089	0.037	0.207	0.114	0.059
40	0.085	0.035	0.013	0.244	0.171	0.076	0.144	0.084	0.041	0.194	0.120	0.054
50	0.078	0.036	0.016	0.298	0.168	0.067	0.149	0.086	0.040	0.189	0.115	0.056

Table 6: Mean integrated squared error (ISE) of RAF estimates across 100 simulation experiments at different shapes, sample size I, and number of basis functions K at the event rate of 50%.

References

- Bach, P., & Klein, N. (2025). Posterior concentration rates for bayesian penalized splines.

 Bayesian Analysis, 1, 1–21.
- Bai, R., Moran, G. E., Antonelli, J. L., Chen, Y., & Boland, M. R. (2022). Spike-and-slab group lassos for grouped regression and sparse generalized additive models. *Journal* of the American Statistical Association, 117, 184–197.
- Berry, G., Gilson, J., Holmes, S., Lewinsohn, H., & Roach, S. (1979). Asbestosis: a study of dose-response relationships in an asbestos textile factory. *Occupational and Environmental Medicine*, 36, 98–112.
- Breslow, N. E., Lubin, J. H., Marek, P., & Langholz, B. (1983). Multiplicative models and cohort analysis. *Journal of the American Statistical Association*, 78, 1–12.
- Claeskens, G., Krivobokova, T., & Opsomer, J. D. (2009). Asymptotic properties of penalized spline estimators. *Biometrika*, 96, 529–544.
- Crainiceanu, C. M., Goldsmith, J., Leroux, A., & Cui, E. (2023). Functional Data Analysis with R. Springer New York, NY, USA.
- Crainiceanu, C. M., Ruppert, D., & Wand, M. P. (2005). Bayesian analysis for penalized spline regression using WinBUGS. *Journal of Statistical Software*, 14, 1–24.
- de Jonge, R., & van Zanten, J. (2012). Adaptive estimation of multivariate functions using conditionally Gaussian tensor-product spline priors. *Electronic Journal of Statistics*,

- 6, 1984 2001. doi: 10.1214/12-EJS735
- Eilers, P. H. C., & Marx, B. D. (1996). Flexible smoothing with B-splines and penalties.

 Statistical Science, 11, 89 121. doi: 10.1214/ss/1038425655
- Gellar, J., Colantuoni, E., Needham, D., & Crainiceanu, C. (2014). Variable-domain functional regression for modeling ICU data. *Journal of American Statistical Association*, 109, 1425-1439.
- Gelman, A. (2006). Prior distributions for variance parameters in hierarchical models (comment on article by Browne and Draper). *Bayesian Analysis*, 1, 515 534. doi: 10.1214/06-BA117A
- Ghosal, S., & van der Vaart, A. (2007). Convergence rates of posterior distributions for noniid observations. *The Annals of Statistics*, 35, 192 223. doi: 10.1214/009053606000001172
- Goeddel, L. A., Hernandez, M., Koffman, L., Murphy, Z., Khanna, A. K., Robich, M., ... Faraday, N. (2024). Fine-mapping the association of acute kidney injury with mean arterial and central venous pressures during coronary artery bypass surgery.

 Anesthesia & Analgesia.
- Harezlak, J., Ruppert, D., & Wand, M. (2018). Semiparametric Regression with R. Springer New York, NY, USA.
- Hastie, T., & Tibshirani, R. (1986). Generalized additive models. Statistical Science, 1, 297 310. doi: 10.1214/ss/1177013604
- Hauptmann, M., Wellmann, J., Lubin, J. H., Rosenberg, P. S., & Kreienbrock, L. (2000).
 Analysis of exposure-time-response relationships using a spline weight function. *Biometrics*, 56, 1105–1108.
- Hu, H., Liu, X., Zheng, Y., He, X., Hart, J., James, P., ... Bian, J. (2023). Methodological challenges in spatial and contextual exposome-health studies. Critical Reviews in Environmental Science and Technology, 53, 827–846. doi: 10.1080/10643389.2022

.2093595

- Jordan T. Johns, V. Z., Ciprian Crainiceanu, & Gellar, J. (2019). Variable-domain functional principal component analysis. *Journal of Computational and Graphical Statistics*, 28, 993–1006.
- Khwaja, A. (2012). KDIGO clinical practice guidelines for acute kidney injury. *Nephron Clinical Practice*, 120, c179–c184.
- Lang, S., & Brezger, A. (2004). Bayesian p-splines. *Journal of computational and graphical statistics*, 13, 183–212.
- Li, Y., & Ruppert, D. (2008). On the asymptotics of penalized splines. *Biometrika*, 95, 415–436.
- Lin, Y., & Zhang, H. H. (2006). Component selection and smoothing in multivariate nonparametric regression. *The Annals of Statistics*, 34, 2272 2297. doi: 10.1214/009053606000000722
- Marra, G., & Wood, S. N. (2011). Practical variable selection for generalized additive models. *Computational Statistics & Data Analysis*, 55, 2372–2387.
- McLean, M., Hooker, G., Staicu, A.-M., Scheipl, F., & Ruppert, D. (2014). Functional generalized additive models. *Journal of Computational and Graphical Statistics*, 23, 249–269.
- Müller, H.-G., & Yao, F. (2008). Functional additive models. *Journal of the American Statistical Association*, 103, 1534–1544.
- Nieuwenhuijsen, M. J. (2003). Exposure assessment in occupational and environmental epidemiology. Oxford University Press. doi: 10.1093/acprof:oso/9780198528616.001
 .0001
- O'Sullivan, F. (1986). A statistical perspective on ill-posed inverse problems (with discussion). Statistical Science, 1, 505–527.
- Panagiotelis, A., & Smith, M. (2008). Bayesian identification, selection and estimation of

- semiparametric functions in high-dimensional additive models. *Journal of Econometrics*, 143, 291-316. doi: https://doi.org/10.1016/j.jeconom.2007.10.003
- Ramsay, J., & Silverman, B. (2005). Functional Data Analysis. Springer New York, NY, USA.
- Ravikumar, P., Lafferty, J., Liu, H., & Wasserman, L. (2009). Sparse additive models.

 *Journal of the Royal Statistical Society Series B: Statistical Methodology, 71, 1009—1030.
- Reiss, P. T., Goldsmith, J., Shang, H. L., & Ogden, R. T. (2017). Methods for scalar-on-function regression. *International Statistical Review*, 85, 228-249.
- Rothman, K., Greenland, S., & Lash, T. (2008). *Modern epidemiology*. Wolters Kluwer Health/Lippincott Williams & Wilkins.
- Ruppert, D., Wand, M., & Carroll, R. (2003). Semiparametric regression. Cambridge University Press.
- Scheipl, F., Fahrmeir, L., & Kneib, T. (2012). Spike-and-slab priors for function selection in structured additive regression models. *Journal of the American Statistical Association*, 107, 1518–1532. doi: 10.1080/01621459.2012.737742
- Schwarz, K., & Krivobokova, T. (2016). A unified framework for spline estimators.

 Biometrika, 103, 121–131.
- Scott, M. J., & APSF Hemodynamic Instability Writing Group. (2024). Perioperative patients with hemodynamic instability: consensus recommendations of the anesthesia patient safety foundation. *Anesthesia & Analgesia*, 138, 713–724.
- Sylvestre, M.-P., & Abrahamowicz, M. (2009). Flexible modeling of the cumulative effects of time-dependent exposures on the hazard. *Statistics in Medicine*, 28, 3437–3453.
- Thomas, D. C. (1988). Models for exposure-time-response relationships with applications to cancer epidemiology. *Annual Review of Public Health*, 9, 451–482.
- Tikhonov, A. (1963). Solution of incorrectly formulated problems and the regularization

- method. Soviet Mathematics Doklady.
- Umlauf, N., Klein, N., & Zeileis, A. (2018). BAMLSS: Bayesian additive models for location, scale, and shape (and beyond). Journal of Computational and Graphical Statistics, 27, 612–627.
- Vacek, P. M. (1997). Assessing the effect of intensity when exposure varies over time. Statistics in Medicine, 16, 505–513.
- Vehtari, A., Gelman, A., & Gabry, J. (2017). Practical bayesian model evaluation using leave-one-out cross-validation and waic. Statistics and Computing, 27, 1413–1432. doi: 10.1007/s11222-016-9696-4
- Wahba, G. (1990). Spline models for observational data. Society for Industrial and Applied Mathematics.
- Wand, M., & Ormerod, J. (2008). On semiparametric regression with O'Sullivan penalized splines. Australian & New Zealand Journal of Statistics, 50, 179 198. doi: 10.1111/j.1467-842X.2008.00507.x
- Wood, S. (2017). Generalized Additive Models: An Introduction with R (2nd ed.). Chapman and Hall/CRC.
- Xiao, L. (2019). Asymptotic theory of penalized splines. *Electronic Journal of Statistics*, 13, 747 794. doi: 10.1214/19-EJS1541
- Xiao, L., Li, Y., Apanasovich, T. V., & Ruppert, D. (2012). Local asymptotics of p-splines. arXiv preprint arXiv:1201.0708.
- Xiao, Y., Abrahamowicz, M., Moodie, E. E., Weber, R., & Young, J. (2014). Flexible marginal structural models for estimating the cumulative effect of a time-dependent treatment on the hazard: reassessing the cardiovascular risks of didanosine treatment in the Swiss HIV cohort study. *Journal of the American Statistical Association*, 109, 455–464.
- Yoo, W. W., & Ghosal, S. (2016). Supremum norm posterior contraction and credible sets

for nonparametric multivariate regression. The Annals of Statistics, 44, 1069–1102.